Electronic Supporting Information (ESI) for ChemComm.

An ultratrace assay of arsenite based on the synergistic quenching effect of $Ru(bpy)_3^{2+}$ and arsenite on the electrochemiluminescence of Au-g-C_3N_4 nanosheets

Ru-Ping Liang,[a] Lu-Dan Yu,[a] Yuan-Jun Tong,[a] Shao-Hua Wen,[a] Shu-Ping Cao[a] and Jian-Ding Qiu*[a,b]

[a] College of Chemistry, Nanchang University, Nanchang 330031, China.

[b] College of Materials and Chemical Engineering, Pingxiang University, Pingxiang 337055, China.

*Corresponding author. Tel/Fax: +86-791-83969518. E-mail: jdqiu@ncu.edu.cn.

Materials. Dicyanamide, tris(2,2'-bipyridyl) ruthenium(II) hexahydrate powder, hydrogen tetrachloroaurate trihydrate ($HAuCl_4 \cdot 3H_2O$), $NaBH_4$, sodium citrate, dithiothreitol (DTT) and poly-diallyldimethylammonium (PDDA) (200000＜MW＜350000, 20% in H_2O) were purchased from Sigma-Aldrich. The 0.1 M pH 7.4 phosphate buffer saline (PBS) solutions were prepared by mixing the stock solution of Na_2HPO_4 and NaH_2PO_4 in appropriate ratio. A solution of 0.1 M pH 7.4 PBS containing 0.1 M $Na_2S_2O_8$ was used as the electrolyte in ECL analysis. Sodium metaarsenite ($NaAsO_2$, As(III)) and sodium arsenate dibasic heptahydrate ($Na_2HAsO_4 \cdot 7H_2O$, As(V)) standard solutions were purchased from National Sharing Platform for Reference Materials (Beijing, China, www.ncrm.org.cn). The Ars-3 sequence with a thoil modification in the 5' terminal: 5'-SH-GGT AAT ACG ACT CAC TAT AGG GAG ATA CCA GCT TAT TCA ATT TTA CAG AAC AAC CAA CGT CGC TCC GGG TAC TTC TTC ATC GAG ATA GTA AGT GCA ATC T-3', was purchased from Shanghai Sangon Biological Engineering Technology & Services Co. Ltd. (Shanghai, China, www.sangon.com). All other chemicals were of analytical grade and used without further purification. Aqueous solutions were prepared with ultrapure water (>18.2 MΩ cm) obtained from a Millipore system.

Apparatus. The ECL measurements were performed on a MPI-B multifunctional electrochemiluminescence analyzer (Xi'an Remex Analytical Instrument Ltd. Co., China). The three-electrode ECL cell was consisted of a modified glassy carbon as the working electrode (φ = 3 mm), an Ag/AgCl (KCl saturated) electrode as the reference, and a platinum wire as the counter electrode. The photomultiplier tube (PMT) was

biased at 700 V, and the scan voltage was from -1.5 to 0 V with the scan rate of 100 mV/s. UV-vis spectra were characterized on an UV-2450 spectrophotometer (Shimadzu, Japan). X-ray photoelectron spectroscopy (XPS) characterizations were measured by a VG Multilab 2000X instrument (Thermal Electron, U.S.A.). Transmission electron microscope (TEM) images were obtained using a JEM-2010 transmission electron microscopy (JEOL, Japan). Cyclic voltammograms (CVs) and electrochemical impedance spectroscopy (EIS) were carried out on an electrochemical workstation (Ivium, Netherlands). CVs were recorded in a potential range between −0.1 V and +0.6 V at a scan rate of 100 mV/s in a solution of 5 mM $K_3[Fe(CN)_6]/K_4[Fe(CN)_6]$ containing 0.1 M KCl. EIS measurements were performed by applying an ac voltage of 5 mV amplitude in 0.01 Hz to 10^6 Hz frequency range. Inductively coupled plasma mass spectrometry (ICP-MS, iCAP Q, Thermo Fisher, America) was used to analyze the real samples.

Synthesis of the g-C_3N_4 NSs. The g-C_3N_4 NSs were prepared following the previously reported literature.[1] Briefly, the bulk carbon nitride was prepared by polymerization of dicyanamide at 550 °C for 4 h under air condition with a ramp of about 3 °C·min^{-1} for heating processes. Then, the ultrathin g-C_3N_4 NSs were synthesized by exfoliating the as-prepared bulk g-C_3N_4 by liquid exfoliation method in water. Briefly, 100 mg of bulk g-C_3N_4 powder was dispersed in 100 mL of water and ultrasound was performed for 16 h. The initial formed suspension was then centrifuged at about 6000 rpm to remove the residual unexfoliated carbon nitride. The mass concentration of the g-C_3N_4 NSs suspension was calculated by weighing the

power dried from a certain volume of the suspension.

Preparation of the Au-g-C_3N_4 NSs. Au-g-C_3N_4 NSs were prepared according to the literature with a slight modification.[2] A 10 μL of 0.01 M $HAuCl_4$ solution was added to 2 mL of the above prepared g-C_3N_4 NSs suspension (ca. 2 mg·mL^{-1}) under stirring. The suspension was sonicated for 10 min, followed by a 2 h stirring at room temperature. This process was repeated 3 times. Afterward, 25 μL of 0.01 M freshly prepared $NaBH_4$ solution was added quickly to the suspension to reduce the $AuCl_4^-$, followed by continuously stirring for 20 min. Then, 10 μL of 0.01 M sodium citrate solution was added dropwise into the above suspension, and the stirring was maintained for 30 min. To remove excess $NaBH_4$, sodium citrate, and unbound gold nanoparticles, the obtained nanohybrid materials were separated by centrifugation, washed thoroughly with water, and finally redispersed in 1 mL of water for further use and characterization.

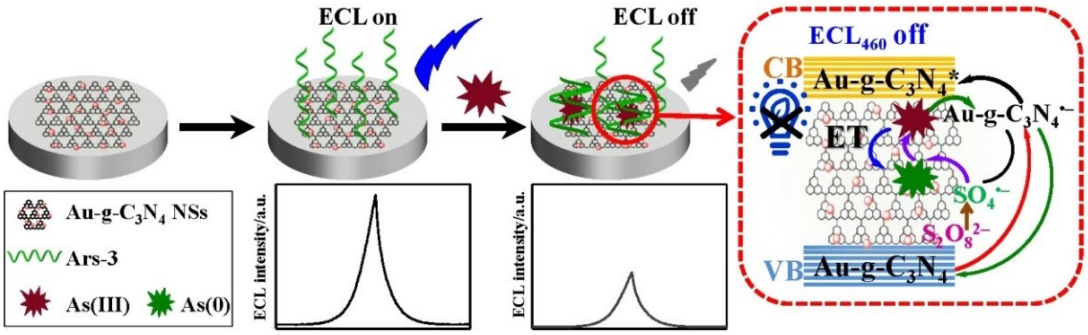

Scheme S1. Illustration and mechanism of single signal ECL biosensor for detection of As(III).

Figure S1 shows the XRD patterns of g-C_3N_4 NSs and Au-g-C_3N_4 NSs. Compared with the characteristic diffraction peak of g-C_3N_4 NSs at 27.2°, Au-g-C_3N_4 NSs show two new diffraction peaks at 38.2° and 44.4° correspond to the (111) and (200) planes of AuNPs, respectively, which further confirms the successful deposition of AuNPs on g-C_3N_4 NSs.

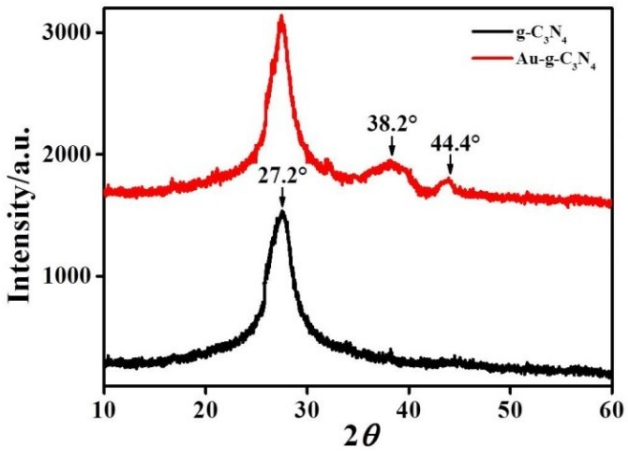

Figure S1. XRD patterns of g-C_3N_4 NSs and Au-g-C_3N_4 NSs.

Figure S2 shows the CD spectra of Ars-3, Ars-3 with As(III), Ars-3 with PDDA, and Ars-3 with PDDA and As(III). Compared with the CD signal of Ars-3,[3] the presence of As(III) results in a significant decrease in both the positive peak at 280 nm and the negative peak at 245 nm. This confirms that As(III) interacts with some bases of Ars-3 and changes its conformation; it restrains the strong p-p* transition of bases with deoxyribose, thus causing a decrease in the CD signal. PDDA is a water-soluble cationic polyelectrolyte that can hybridize with single-strand DNA due to the electrostatic interaction between the positively charged cationic polymers and negatively charged phosphate backbone of DNA.[3] However, this electrostatic interaction between PDDA and Ars-3 will not affect the original

conformation of Ars-3, since PDDA would bind to the negatively charged phosphate backbone rather than the bases of the Ars-3. When PDDA hybridizes with Ars-3, the loading of $Ru(bpy)_3^{2+}$ adsorbed on PDDA/Ars-3/Au-g-C_3N_4/GCE is very low. The addition of As(III) decreased the CD signals of the Ars-3 with no change in the peak locations, which proves that PDDA had no effect on the recognition of Ars-3 and As(III).

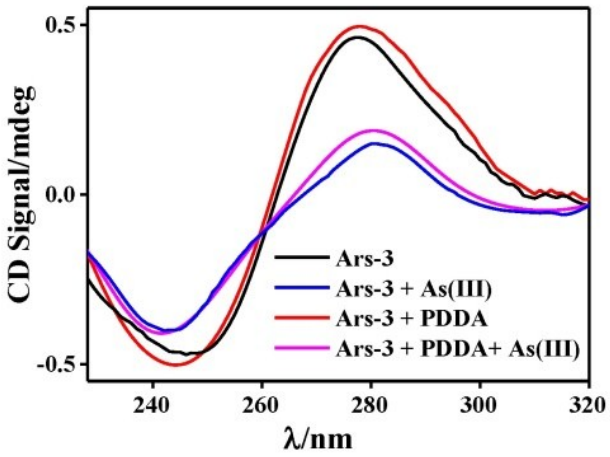

Figure S2. CD spectra of Ars-3, Ars-3 with As(III), Ars-3 with PDDA, and Ars-3 with PDDA and As(III).

Quenching Mechanism of As(III) to Au-g-C_3N_4 NSs. The ECL emission of Au-g-C_3N_4 is generated by a chemical reaction triggered by the electrochemical reaction in the potential from 0 to –1.5 V, and As(III) is reduced to As(0) at the electrode at the potentials.[4-6] Since the redox potential of As(III)/As(0) (0.248 V) lies between the conduction band (−0.83 V) and the valence band (1.83 V) of the g-C_3N_4 NSs, efficient electron transfer from the Au-g-$C_3N_4^{\bullet-}$ to As(III) can occur.[7] Thus, the electrochemically generated As(0) can consume $SO_4^{\bullet-}$ to produce As(III), and meanwhile, As(III) can efficiently oxidize Au-g-$C_3N_4^{\bullet-}$ to form ground state Au-g-

C_3N_4. Both $SO_4^{\bullet-}$ and Au-g-$C_3N_4^{\bullet-}$ are important species for the formation of excited state Au-g-C_3N_4*; such simultaneous consumption of $SO_4^{\bullet-}$ and Au-g-$C_3N_4^{\bullet-}$ would greatly decrease the amount of Au-g-C_3N_4*, leading to the effective decrease in the ECL signal of the Au-g-C_3N_4 NSs (equ (S1)–(S7)). The quenching effect of As(III) on the cathodic ECL at Au-g-C_3N_4 modified electrode can be attributed to electron transfer. The electron transfer process can be expressed as follows:

$$As(III) + e \longrightarrow As(0) \quad (S1)$$

$$\text{Au-g-}C_3N_4 + e \longrightarrow \text{Au-g-}C_3N_4^{\bullet-} \quad (S2)$$

$$S_2O_8^{2-} + e \longrightarrow SO_4^{\bullet-} + SO_4^{2-} \quad (S3)$$

$$SO_4^{\bullet-} + As(0) \longrightarrow SO_4^{2-} + As(III) \quad (S4)$$

$$\text{Au-g-}C_3N_4^{\bullet-} + As(III) \longrightarrow \text{Au-g-}C_3N_4 + As(0) \quad (S5)$$

$$\text{Au-g-}C_3N_4^{\bullet-} + SO_4^{\bullet-} \longrightarrow \text{Au-g-}C_3N_4^{*} + SO_4^{2-} \quad (S6)$$

$$\text{Au-g-}C_3N_4^{*} \longrightarrow \text{Au-g-}C_3N_4 + hv \quad (S7)$$

When the potential is scanned from −1.5 to 0 V, As(III) can be reduced to As(0) at the electrode (S1), meanwhile, Au-g-C_3N_4 and the coreactant $S_2O_8^{2-}$ are simultaneously reduced to Au-g-$C_3N_4^{\bullet-}$ and $SO_4^{\bullet-}$ on electrode surface (S2-S3). The electrochemically generated As(0) can consume $SO_4^{\bullet-}$ to produce oxidation state As(III) (S4), and meanwhile As(III) can efficiently oxidize the Au-g-$C_3N_4^{\bullet-}$ to form ground state Au-g-C_3N_4 (S5). Both $SO_4^{\bullet-}$ and Au-g-$C_3N_4^{\bullet-}$ are important species for the formation of excited state Au-g-C_3N_4* (S6), such simultaneous consumption of $SO_4^{\bullet-}$ and Au-g-$C_3N_4^{\bullet-}$ would greatly decrease the amount of the Au-g-C_3N_4*, leading to the effective quenching of the ECL signal of Au-g-C_3N_4 (S7).

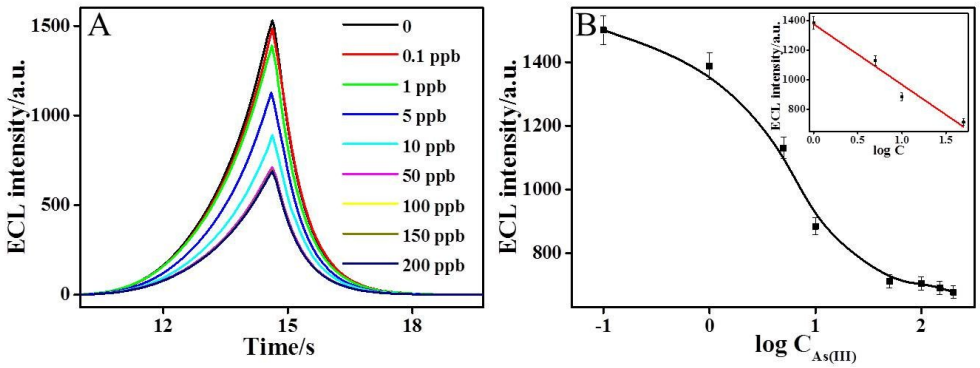

Figure S3. (A) ECL curves at 460 nm of the biosensor at different concentrations of As(III) (from a to i: 0, 0.1, 1, 5, 10, 50 ppb, 100 ppb, 150 ppb and 200 ppb respectively). (B) Relationship between the intensity of ECL and $\log C_{As(III)}$. Inset: Linear relation of the intensity of ECL and $\log C_{As(III)}$. The detection was performed in 0.1 M pH 7.4 PBS solution containing 0.1 M $Na_2S_2O_8$. Scan rate: 100 mV/s. Scan range: −1.5 V ~ 0 V. PMT: 700 V.

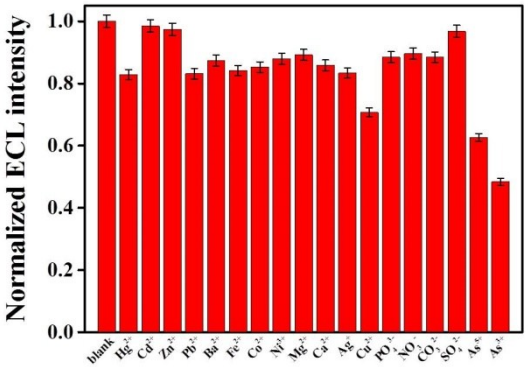

Figure S4. ECL responses for different arsenic species and selectivity of the ECL assay over heavy metal ions and oxygen anion. The concentration of As(III) was 50 ppb and the concentrations of the metal ions were 500 ppb.

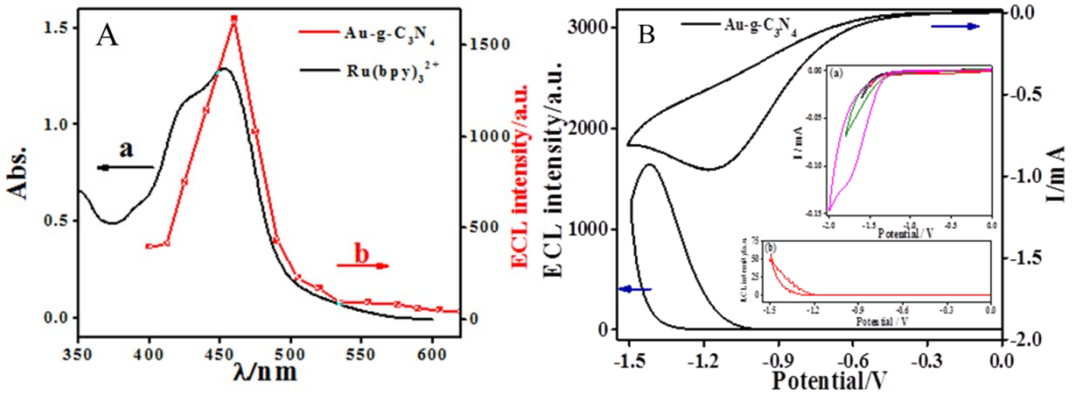

Figure S5. (A) UV−vis spectrum of $Ru(bpy)_3^{2+}$ and ECL spectrum of Au-g-C_3N_4 NSs. (B) CVs and ECL signal of Au-g-C_3N_4 NSs, inset (a) is the CVs of $Ru(bpy)_3^{2+}$ and inset (b) is the ECL signal of $Ru(bpy)_3^{2+}$.

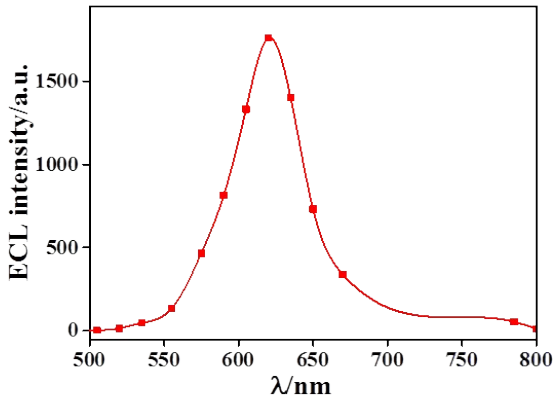

Figure S6. ECL spectrum of $Ru(bpy)_3^{2+}$.

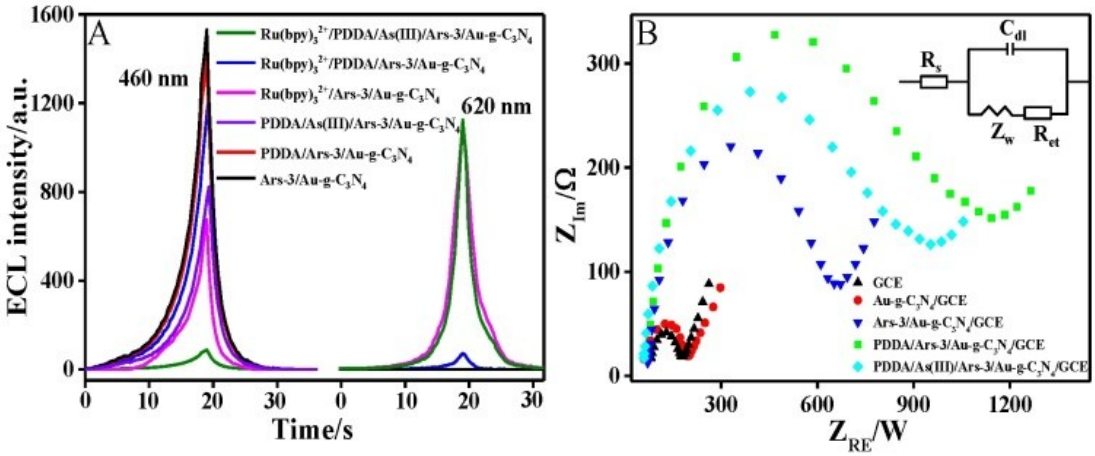

Figure S7. (A) ECL intensities of Ars-3/Au-g-C_3N_4/GCE, PDDA/Ars-3/Au-g-C_3N_4/GCE, PDDA/As(III)/Ars-3/Au-g-C_3N_4/GCE, $Ru(bpy)_3^{2+}$/Ars-3/Au-g-C_3N_4/GCE, $Ru(bpy)_3^{2+}$/PDDA/Ars-3/Au-g-C_3N_4/GCE, and $Ru(bpy)_3^{2+}$/PDDA/As(III)/Ars-3/Au-g-C_3N_4/GCE. The concentration of As(III) was 10 ppb. (B) EIS spectra of GCE, Au-g-C_3N_4/GCE, Ars-3/Au-g-C_3N_4/GCE, PDDA/Ars-3/Au-g-C_3N_4/GCE, and PDDA/As(III)/Ars-3/Au-g-C_3N_4/GCE in a 0.1 M PBS solution (pH 7.4) containing 5 mM $[Fe(CN)_6]^{3-/4-}$ and 0.1 M KCl. Inset: the equivalent circuit used to model the impedance data. R_s, Z_w, and C_{dl} represent the solution resistance, the Warburg diffusion resistance, and the double-layer capacitance, respectively.

Quenching Mechanism of $Ru(bpy)_3^{2+}$ to Au-g-C_3N_4 NSs. The quenching effect of $Ru(bpy)_3^{2+}$ on the cathodic ECL at Au-g-C_3N_4 modified electrode can be attributed to ECL resonance energy transfer (ECL-RET). The ECL-RET process can be expressed as follows:

$$\text{Au-g-}C_3N_4 + e \longrightarrow \text{Au-g-}C_3N_4^{\bullet -} \quad \text{(S8)}$$

$$S_2O_8^{2-} + e \longrightarrow SO_4^{\bullet -} + SO_4^{2-} \quad \text{(S9)}$$

$$\text{Au-g-}C_3N_4^{\bullet -} + SO_4^{\bullet -} \longrightarrow \text{Au-g-}C_3N_4^{*} + SO_4^{2-} \quad \text{(S10)}$$

$$\text{Au-g-}C_3N_4^{*} + Ru(bpy)_3^{2+} \longrightarrow \text{Au-g-}C_3N_4 + Ru(bpy)_3^{2+*} \quad \text{(S11)}$$

$$Ru(bpy)_3^{2+*} \longrightarrow Ru(bpy)_3^{2+} + h\nu \quad \text{(S12)}$$

When the potential is scanned from −1.5 to 0 V, Au-g-C_3N_4 and $S_2O_8^{2-}$ are simultaneously reduced to Au-g-$C_3N_4^{\bullet -}$ and $SO_4^{\bullet -}$ on electrode surface (equ S8-S9). The strong oxidant $SO_4^{\bullet -}$ can react with Au-g-$C_3N_4^{\bullet -}$ to form excited state Au-g-C_3N_4* (S10). As the donor of ECL-RET system, Au-g-C_3N_4* can transfer energy to $Ru(bpy)_3^{2+}$ to form $Ru(bpy)_3^{2+*}$ (S11),[8] and the formed $Ru(bpy)_3^{2+*}$ would return to the ground state with light emitting at 620 nm (S12), thus, resulting in a decreased ECL signal of Au-g-C_3N_4 and a strong ECL signal of $Ru(bpy)_3^{2+}$.

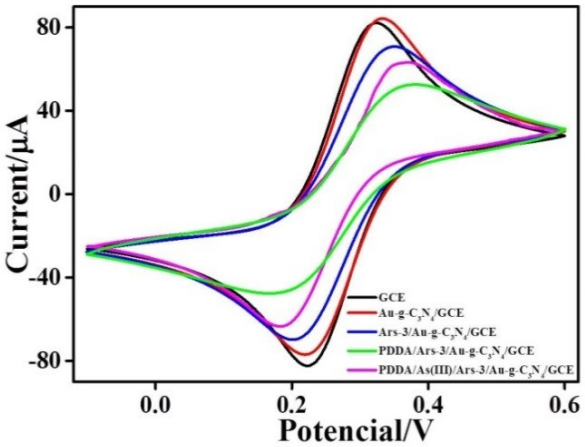

Figure S8. CV curves of GCE, Au-g-C_3N_4/GCE, Ars-3/Au-g-C_3N_4/GCE, PDDA/Ars-3/Au-g-C_3N_4/GCE, and PDDA/As(III)/Ars-3/Au-g-C_3N_4/GCE in a 0.1 M PBS solution (pH 7.4) containing 5 mM $[Fe(CN)_6]^{3-/4-}$ and 0.1 M KCl.

Optimization of Detection Conditions. To apply the ECL system to As(III) monitoring efficiently, the experimental parameters including the concentration of Ars-3, binding time of As(III) and Ars-3, and pH of the reaction solution were optimized. As shown in Figure S9A, the value of ECL_{620}/ECL_{460} increased with the increasing Ars-3 concentration up to 100 nM, then declined when further increased the concentration of Ars-3. Thus, 100 nM Ars-3 was selected for sensor preparation. The reaction time between Ars-3 and As(III) greatly influenced the response. The value of ECL_{620}/ECL_{460} increased gradually with increasing reaction time and reached a plateau at the reaction time of 30 min (Figure S9B). Therefore, 30 min was selected for the reaction in the detection of As(III). As shown in Figure S9C, the value of ECL_{620}/ECL_{460} increased with the increasing pH value up to 7.4 then declined when further increased the pH of the reaction solution. So, pH 7.4 was chosen as the optimized pH of the reaction solution.

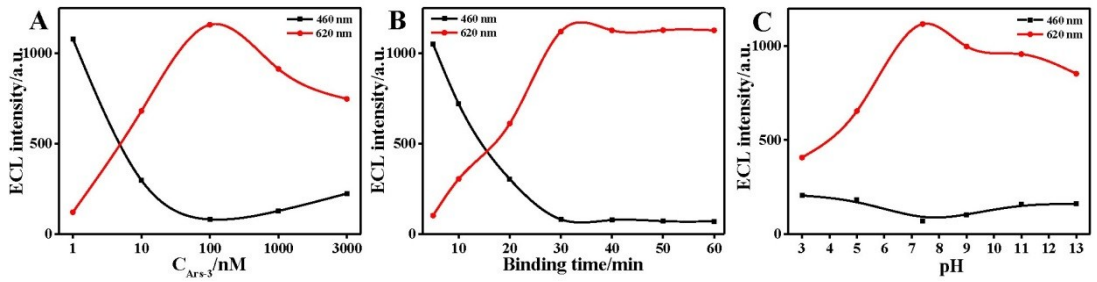

Figure S9. Effects of (A) concentration of Ars-3, (B) binding time of As(III) and Ars-3, and (C) solution pH on the ECL intensity of Au-g-C_3N_4 at 460 nm and $Ru(bpy)_3^{2+}$ at 620 nm. The concentration of As(III) was 10 ppb.

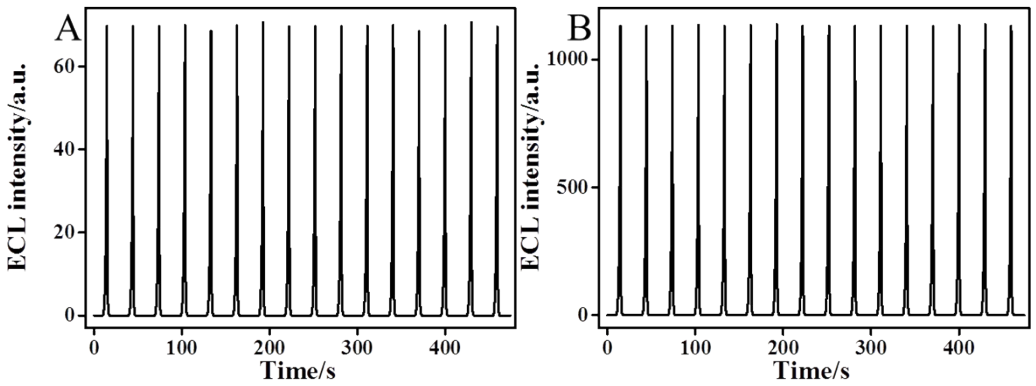

Figure S10. ECL intensity-time curves of the biosensor at (A) 460 nm and (B) 620 nm for 10 ppb As(III).

Table S1. Comparison of the performance between the proposed sensor and other methods for As(III) detection

Methods	Materials	LOD (ppb)	Linear range (ppb)	Ref.
Colorimetry	Aptamer, PDDA, AuNPs	5.3	5–3000	3
Colorimetry	G/T-rich ssDNA, AuNPs	0.5	5-2000	9
Colorimetry	Citrate-gold NPs	1.8	4-100	10
DLS	GSH/DTT/Cys-AuNPs	0.003	0.001-50	11
Fluorescence	Cys-Gold NCs	4.04	376-8646	12
Fluorescence	QDs-CDs test paper	1.5	5-100	13
SERS	GSH/4-MPY-AgNPs	0.76	4-300	14
SERS	Aptamer, Au@Ag NP	0.1	0.5-10	15
ASV	Au-Pd/GCE	0.25	1-25	16
SWASV	$MnFe_2O_4$/Au-GCE	1.95	10-100	17
SWASV	Au@Fe_3O_4-RTIL/SPCE	0.0022	0.1-1	4
SWASV	AuNPs/α-MnO_2/GCE	0.019	1-10	5
SWASV	Fe_3O_4-RTIL/SPCE	0.0008	1−10	6
DPV	Aptasensor, PDDA	0.0113	0.015-7.5	18
DPV	Aptasensor, PDDA	0.5	0.5-10	19
DPV	RuOx NPs-GCE	0.1	0.6-56	20
DPV	SBP DNA, MB	0.075	0.1-200	21
EIS	ArsSApt/Au electrode	0.1	50-10000	22
ECL	Au-g-C_3N_4/Aptamer/$Ru(bpy)_3^{2+}$	7×10^{-7}	10^{-6}-10	This work

Table S2. Evaluation of monitoring As(III) pollution in different real water samples

Samples	Added(ppb)	Found(ppb)	Recovery(%)	RSD(%)	ICP-MS(ppb)	Related error(%)
Tap water 1	0	0.001	-	4.5	0	-
Tap water 2	0.05	0.048	94	4.1	0.05	4.0
Tap water 3	0.5	0.511	101.8	3.7	0.54	5.3
Tap water 4	5	5.082	101.4	3.2	4.88	-4.1
River water 1	0	0.871	-	4.3	0.95	8.3
River water 2	0.05	0.924	106	4.1	0.97	4.7
River water 3	0.5	1.358	97.4	3.9	1.31	-3.5
River water 4	5	5.925	101.1	2.7	6.05	2.1
Lake water 1	0	0.743	-	4.6	0.72	3.2
Lake water 2	0.05	0.791	96	4.3	0.83	4.7
Lake water 3	0.5	1.284	108.2	3.7	1.22	-5.2
Lake water 4	5	5.66	98.3	3.1	5.45	-3.9

References

1 X. Zhang, X. Xie, H. Wang, J. Zhang, B. Pan, Y. Xie, *J. Am. Chem. Soc.*, 2013, **135**, 18-21.

2 L. Chen, X. Zeng, P. Si, Y. Chen, Y. Chi, D.H. Kim, G. Chen, *Anal. Chem.*, 2014, **86**, 4188-4195.

3 Y. Wu, S. Zhan, F. Wang, L. He, W. Zhi, P. Zhou, *Chem. Commun.*, 2012, **48**, 4459-4461.

4 J. Wei, S.-S. Li, Z. Guo, X. Chen, J.-H. Liu, X.-J. Huang, *Anal. Chem.*, 2016, **88**, 1154-1161.

5 M. Yang, X. Chen, T.-J. Jiang, Z. Guo, J.-H. Liu, X.-J. Huang, *Anal. Chem.*, 2016, **88**, 9720-9728.

6 C. Gao, X.-Y. Yu, S.-Q. Xiong, J.-H. Liu, X.-J. Huang, *Anal. Chem.*, 2013, **85**, 2673-2680.

7 C. Cheng, Y. Huang, X. Tian, B. Zheng, Y. Li, H. Yuan, D. Xiao, S. Xie, M. M. Choi, *Anal. Chem.*, 2012, **84**, 4754-4759.

8 Q. M. Feng, Y. Z. Shen, M. X. Li, Z. L. Zhang, W. Zhao, J. J. Xu, H. Y. Chen, *Anal. Chem.*, 2016, **88**, 937-944.

9 R.-P. Liang, Z.-X. Wang, L. Zhang, J.-D. Qiu, *Chem. Eur. J.*, 2013, **19**, 5029-5033.

10 L. Gong, B. Du, L. Pan, Q. Liu, K. Yang, W. Wang, H. Zhao, L. Wu, Y. He, *Microchim. Acta*, 2017, **184**, 1185-1190.

11 J. R. Kalluri, T. Arbneshi, S. Afrin Khan, A. Neely, P. Candice, B. Varisli, M. Washington, S. McAfee, B. Robinson, S. Banerjee, A. K. Singh, D. Senapati, P. C. Ray, *Angew. Chem. Int. Ed.*, 2009, **121**, 9848-9851.

12 S. Roy, G. Palui, A. Banerjee, *Nanoscale*, 2012, **4**, 2734-2740.

13 Y. Zhou, X. Huang, C. Liu, R. Zhang, X. Gu, G. Guan, C. Jiang, L. Zhang, S. Du, B. Liu, M.-Y. Han, Z. Zhang, *Anal. Chem.*, 2016, **88**, 6105-6109.

14 J. Li, L. Chen, T. Lou, Y. Wang, *ACS Appl. Mater. Interfaces*, 2011, **3**, 3936-3941.

15 L. Song, K. Mao, X. Zhou, J. Hu, *Talanta*, 2016, **146**, 285-290.

16 Y. Lan, H. Luo, X. Ren, Y. Wang, Y. Liu, *Microchim. Acta*, 2012, **178**, 153-161.

17 S.-F. Zhou, X.-J. Han, H.-L. Fan, Q.-X. Zhang, Y.-Q. Liu, *Electrochim. Acta.,* 2015, **174**, 1160-1166.

18 L. Cui, J. Wu, H. Ju, *Biosens. Bioelectro.*, 2016, **79**, 861-865.

19 Y. Wang, P. Wang, Y. Wang, X. He, K. Wang, *Talanta*, 2015, **141**, 122-127.

20 R. Gupta, J. S. Gamare, A. K. Pandey, D. Tyagi, J. V. Kamat, *Anal. Chem.*, 2016, **88**, 2459-2465.

21 S. Wen, C. Zhang, R. Liang, B. Chi, Y. Yuan, J. Qiu, *Microchim. Acta*, 2017, **184**, 4047-4054.

22 K. Vega-Figueroa, J. Santillán, V. Ortiz-Gómez, E. O. Ortiz-Quiles, B. A. Quiñones-Colón, D. A. Castilla-Casadiego, J. Almodóvar, M. J. Bayro, J. A. Rodríguez-Martínez, E. Nicolau, *ACS Omega*, 2018, **3**, 1437-1444.